MODELING OF UNSTEADY BLADE SHEET AND DEVELOPED TIP VORTEX CAVITATION

Hanseong Lee and Spyros A. Kinnas

The University of Texas at Austin, Austin, TX 78712, USA

Abstract

A boundary element method is used for the numerical modeling of unsteady blade sheet and developed tip vortex cavitation on propellers. The objective of this work is to predict more accurately blade sheet and developed tip vortex cavity in the vicinity of the blade tip subject to a non-axisymmetric flow-field. The ultimate goal of this work is to predict more accurately the hull pressures induced by the unsteady cavities on the blade and tip. Initially, we assume that the section of the tip vortex cavity shape is circular and the wake a pure helical surface without contraction and roll-up. Once the fully wetted problem is solved by applying the potential based panel method on the assumed tip vortex cavity and wake geometry, the three-component velocities on the tip vortex cavity are calculated by numerically differentiating the velocity potential, and those on the wake surface are determined from the differentiated Green's formula. The new wake surface and the trajectory of the tip vortex cavity core are determined by aligning the wake surface with the flow velocity, in fully unsteady manner. Once the aligned wake surface is determined in an iterative way, the shape of the blade sheet and tip vortex cavity, having a constant pressure distribution, is determined by applying the dynamic and the kinematic boundary conditions on the cavity surface. The method is applied in the case of simplified 2-D vortex cavity, 3-D elliptic wing, and propeller blades subject to inclined and non-axisymmetric inflows. Comparisons with experiments in terms of unsteady cavity shapes, tip vortex cavity trajectories, and unsteady blade forces, are finally presented.

1 Introduction

A marine propeller is often operating in a non-axisymmetric flow field and thus its blades are subject to an unsteady flow field. Depending on operating conditions, such as ship speed, propeller submergence depth, rotational velocity of propeller, and ship maneuvering conditions, the propeller can experience cavitation. The most destructive effect of cavitation occurs when a grown cavity collapses on the propeller surface. Excessive pressures during the collapse stage cause pitting of the blades and accelerate blade erosion. In addition, the hydrodynamic phenomenon of the rapid growth and the collapse of the cavity can produce severe pressure fluctuations on the adjacent hull, as well as radiated noise. Therefore, the development of a computational method which is capable of predicting propeller performance, including cavitation, accurately, is essential in the design process.

The boundary element (or panel) method has been applied successfully to the prediction of propeller performance in steady and unsteady non-cavitating conditions. A potential based panel method for the prediction of partial and super cavitation on 2-D hydrofoils was developed by Kinnas and Fine (1990). This method was finally extended for the prediction of unsteady sheet cavitation on propellers in non-linear theory (Kinnas and Fine (1992)). The modeling of face and mid-chord cavitation was developed by Mueller and Kinnas (1999), in which face and back cavitation was detected separately, and this work was extended recently by Young and Kinnas (2001), where both face and back cavitation with the search of mid-chord detachment can be predicted simultaneously. Kinnas et al. (1998) developed a potential based panel method to predict the shape of a tip vortex cavity far downstream in the case of a horseshoe, and obtained a pressure on the cavity surface which was constant and equal to the specified vapor pressure.

Tip vortex cavitation inception is strongly dependent on the viscous flow in the vortex core, and has been studied experimentally extensively (McCormick (1962), Stinebring et al. (1991), Fruman (1994), and Arndt et al. (1991)). Numerical methods, based on Reynolds-Averaged Navier-Stokes equations, have attempted to predict the minimum pressure in the core of a 3-D tip vortex. These methods however, have been hampered by the fact that they cannot take into account the unsteadiness of the core pressures (which is suppressed by the Reynolds averaging), the water quality, and the nuclei content, all of which have been found to affect the inception conditions drastically (Fruman (1994)). In the present work we will assume that the tip vortex cavity is *fully developed* and that the flow outside the tip vortex cavity is inviscid.

There has been a lot of research on wake alignment techniques to predict more accurately propeller performance in uniform inflow. The effect of wake geometry on the predicted propeller torque and thrust was first investigated by Kerwin and Lee (1978). Greeley and Kerwin (1982) developed an iterative procedure to determine the wake geometry of a propeller using vortex lattice method, in which the roll-up of vortex sheet was modeled with one helical vortex line from each blade. The propeller unsteady forces due to the inclined inflows was experimentally investigated by Boswell et al. (1984). Kinnas and Pyo (1999) extended the method of Greeley and Kerwin (1982) in the case of inclined inflows by essentially aligning the wake by using a uniform transverse velocity which was equal to the projection of the inflow to the propeller plane.

It is well known that the trailing wake sheet traveling downstream of the blade experiences contraction and roll-up at the tip regions. In the past, the wake contraction and vortex roll-up motion were determined from measurements by using Laser Doppler Velocimetry(LDV) or more recently Particle Image Velocimetry(PIV) systems. These measurements were used to adjust simplified techniques which determine the location of the trailing wake sheet. Since the roll-up and the contraction of vortex depend on the propeller operating conditions and the geometric characteristics, the range in which the experimental measurements are applicable to the numerical calculation is confined to the near design condition of propeller. More recently, the accurate prediction of wake geometry which rolls-up and contracts as it travels from the blade trailing edge has been achieved by aligning the wake surface with the local total velocities, *i.e.* by applying the force-free condition on the wake surface. Since the trajectory of a tip vortex in non-cavitating conditions has been found to be close enough to that of cavitating conditions (Arndt et al. (1991)), the wake alignment in non-cavitating flow can also be used to predict the trajectory of the cavitating tip vortex.

In this paper, the formulation and boundary conditions for the blade sheet cavity and tip vortex cavity, as well as the algorithm for the fully unsteady wake alignment are summarized. Numerical results using the described method are presented and compared with those of other methods, as well those measured in experiments.

2 Formulation

2.1 Governing equation

Consider a propeller which rotates at a constant angular velocity $\vec{\omega}$ and is subject to a non-axisymmetric inflow $\vec{U}_w(x,r,\theta)$ [1]. The geometry and the coordinate systems are shown in Figure 1. The solution is determined in the (x,y,z) coordinate system, which is rotating with the propeller. Then, the total inflow velocity relative to the propeller is

$$\vec{U}_{in}(x,y,z,t) = \vec{U}_w(x,r,\theta-\omega t) + \vec{\omega}\times\vec{x}(x,y,z) \tag{1}$$

where $r=\sqrt{y^2+z^2}$ and $\theta=\tan^{-1}(z/y)$.

The fluid is assumed to be inviscid, and the flow to be incompressible and irrotational. Then, the fluid domain can be represented by using the time-dependent perturbation potential $\phi(x,y,z,t)$ defined as follows:

$$\vec{q}(x,y,z,t) = \vec{U}_{in}(x,y,z,t) + \nabla\phi(x,y,z,t) \tag{2}$$

where $\vec{q}(x,y,z,t)$ is the time dependent total flow velocity. The perturbation potential $\phi(x,y,z,t)$ defined in Eqn. (2) has to satisfy Laplace's equation, $\nabla^2\phi=0$. The potential ϕ_p at arbitrary point, p, on the body must satisfy the Green's third identity.

$$2\pi\phi_p(t) = \iint_{S_B+S_T+S_C}\left[\phi_q(t)\frac{\partial G(p;q)}{\partial n_q(t)} - \frac{\partial\phi_q(t)}{\partial n_q(t)}G(p;q)\right]dS + \iint_{S_w}\Delta\phi_w(r_q,\theta_q,t)\frac{\partial G(p;q)}{\partial n_q(t)}dS \tag{3}$$

[1] Inflow $\vec{U}_w(x,r,\theta)$ is assumed to be effective wake, *i.e.* it includes the interaction between the vorticity in the inflow and the propeller (Choi and Kinnas (2000))

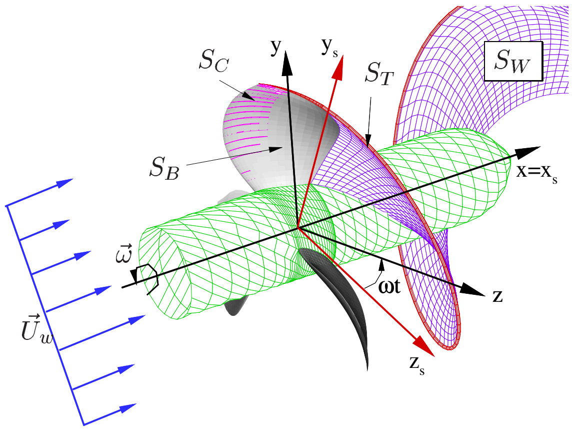

Figure 1: Propeller, developed tip vortex cavity, and trailing wake geometry

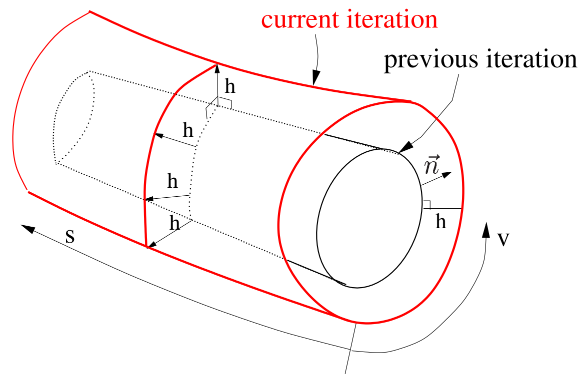

Figure 2: Schematic of kinematic condition on tip vortex cavity surface

where $G(p;q) = 1/R(p;q)$ is the infinite domain Green's function, and $R(p;q)$ is the distance between the field point p and the variable point q. $\vec{n}_q(t)$ is the unit normal vector to the surface of the propeller, the cavity and the wake, and points into the fluid domain. $\Delta\phi_w$ is the potential jump across the wake surface S_w. Also, S_B, S_T and S_C denote fully wetted blade, tip vortex cavity and blade sheet cavity surfaces, respectively.

Eqn. (3) implies that the solution potential $\phi_p(t)$ on the body surface can be expressed by distributing sources and dipoles over the blade and the cavity surfaces, and only the dipoles on the wake surface.

2.2 Boundary conditions

The exact potential solution of Eqn. (3) can be uniquely determined when the boundary conditions are applied to the exact body boundaries and fluid domain. These boundary conditions are as follows:

- The flow tangency condition : the fluid flow is tangent to the propeller blades and cavity surfaces.

$$\frac{\partial \phi(x,y,z,t)}{\partial n} = -\vec{U}_{in}(x,y,z,t)\cdot\vec{n} \tag{4}$$

- The blade sheet cavity closure condition : The cavity thickness at the end of partial or super cavities should be equal to zero.

- The dynamic boundary condition on the cavity surface : The pressure inside or on the cavity surface is constant and equal to the cavitating pressure p_c. The cavitating pressure on the propeller surface can be derived by using Bernoulli's equation with respect to the propeller fixed coordinate system.

$$\frac{p_o}{\rho} + \frac{1}{2}|\vec{U}_w|^2 = \frac{\partial\phi}{\partial t} + \frac{p_c}{\rho} + \frac{1}{2}|\vec{q}_t|^2 - \frac{1}{2}\omega^2 r^2 + g y_d \tag{5}$$

where ρ is the fluid density, r is the distance from the axis of rotation and $\vec{q}_t$ is the total velocity on the cavity surface. p_o is the pressure far upstream on the shaft axis. Also, g is the gravitational acceleration and y_d is the vertical distance from the axis of rotation. y_d is defined to be negative in the direction of gravity.

Since the position of the exact cavity surface which satisfies the kinematic boundary condition is unknown, the source strength $(\frac{\partial\phi}{\partial n})$ in Eqn. (3) is also unknown. Since either the source or the dipole strength has to be known in order to solve the Green's formula, the dipole strength on the cavity surface should be determined using the dynamic boundary condition.

By using Eqn. (5) and the expression for the magnitude of total velocity on the local non-orthogonal coordinate system, the following quadratic equation can be obtained:

$$\begin{aligned}\left(\frac{\partial\phi}{\partial s}+U_s\right)^2 &- 2\left(\frac{\partial\phi}{\partial s}+U_s\right)\left(\frac{\partial\phi}{\partial v}+U_v\right)\cos\theta+\left(\frac{\partial\phi}{\partial v}+U_v\right)^2 \\ &- \sin^2\theta\left(n^2D^2\sigma_n+|\vec{U}_w|^2+\omega^2r^2-2gy_d-2\frac{\partial\phi}{\partial t}\right)=0\end{aligned} \tag{6}$$

where the cavitation number, σ_n, is defined as $\sigma_n = \frac{p_o-p_c}{\frac{\rho}{2}n^2D^2}$, n and D are rotational frequency (revolutions per second) and diameter of propeller, respectively. Also, the local inflow velocities on the local coordinate system are given by

$$U_s = \vec{U}_{in}\cdot\vec{s} \quad , \quad U_v = \vec{U}_{in}\cdot\vec{v} \quad , \quad U_n = \vec{U}_{in}\cdot\vec{n} \tag{7}$$

The solution of Eqn. (6) can be obtained with respect to either $\frac{\partial\phi}{\partial v}$, or $\frac{\partial\phi}{\partial s}$, depending on how we wish to integrate the perturbation velocity in order to get the potential. In the case of blade cavity, we chose to solve with respect to $\frac{\partial\phi}{\partial s}$ since $\frac{\partial\phi}{\partial v}$ is not expected to have a large effect on the solution(Fine (1992)). The equation for the perturbation velocity $\frac{\partial\phi}{\partial s}$ can be obtained as a solution to a quadratic equation, where the negative solution is excluded since the flow on the surface has to be pointing in the downstream direction.

The potential on the partial cavity surface is obtained by integrating the solution ($\frac{\partial\phi}{\partial s}$) of Eqn. (6).

$$\begin{aligned}\phi(s,v,t) &= \phi(0,v,t)+\int_0^s\left[-U_s+(\frac{\partial\phi}{\partial v}+U_v)\cos\theta\right. + \\ &+ \left.\sin\theta\sqrt{n^2D^2\sigma_n+|\vec{U}_w|^2+\omega^2r^2-2gy_d-2\frac{\partial\phi}{\partial t}-(\frac{\partial\phi}{\partial v}+U_v)^2}\right]ds\end{aligned} \tag{8}$$

The unknowns, $\frac{\partial\phi}{\partial v}$ and $\frac{\partial\phi}{\partial t}$, are treated as knowns and will be evaluated in an iterative way (Fine (1992), Kinnas and Fine (1992)). Another unknown, $\phi(0,v,t)$, is determined as a function of the potentials on the wetted part of the propeller surface.

Since the cross flow term (tangential velocity) on the tip vortex cavity is dominant and cannot be neglected, the potential on the tip vortex cavity is determined by solving Eqn. (6) with respect to $\frac{\partial\phi}{\partial v}$ and integrating $\frac{\partial\phi}{\partial v}$ along v-direction.

$$\begin{aligned}\phi(s,v,t) &= \phi(s,0,t)+\int_0^v\left[-U_v+(\frac{\partial\phi}{\partial s}+U_s)\cos\theta\right. + \\ &+ \left.\sin\theta\sqrt{n^2D^2\sigma_n+|\vec{U}_w|^2+\omega^2r^2-2gy_d-2\frac{\partial\phi}{\partial t}-(\frac{\partial\phi}{\partial s}+U_s)^2}\right]ds\end{aligned} \tag{9}$$

Also, the unknowns, $\frac{\partial\phi}{\partial s}$ and $\frac{\partial\phi}{\partial t}$, are evaluated iteratively in a similar way. The unknown $\phi(s,0,t)$ at the tip vortex can be determined by applying Eqn. (8) at the intersection of the tip vortex cavity with the trailing wake.

- The kinematic condition on the cavity surface : A fluid particle on the cavity surface has to be remain on that surface, *i.e.*, the substantial derivative of a function for the cavity surface has to be zero.

$$\frac{DF(x,y,z,t)}{Dt} = \frac{\partial F(x,y,z,t)}{\partial t}+\vec{q}_t(x,y,z,t)\cdot\nabla F(x,y,z,t)=0 \tag{10}$$

where $F(x,y,z,t)=n-h(s,v,t)$ is a function expressing the cavity surface, $\vec{q}_t$ is the total velocity on the cavity surface, and h and n are defined as the radius increment normal to the tip vortex cavity surface of previous iteration and the normal coordinate, respectively, as shown in Figure 2.

Once the Green's formula which satisfies the boundary conditions is inverted, this kinematic boundary condition is used to determine the location of the cavity surface. The application of the kinematic boundary condition to find the position of the partial and the super cavity surface has been discussed in detail by Fine (1992), and Kinnas and Fine (1992), and will not be described here. The kinematic condition on the tip vortex cavity surface can be derived in a similar way. Figure 2 shows the definition of geometry of tip vortex cavity shape and its new coordinate normal to the original coordinate. By substituting the function expressing the cavity surface, $F(x, y, z, t) = n - h(s, v, t)$, the velocity gradient in a non-orthogonal coordinate system into Eqn. (10), the partial differential equation for the radius increment of tip vortex cavity can be obtained as follows.

$$\frac{\partial h}{\partial s}(V_s - V_v \cos\theta) + \frac{\partial h}{\partial v}(V_v - V_s \cos\theta) = \sin^2\theta(V_n - \frac{\partial h}{\partial t}) \tag{11}$$

where

$$V_s = U_s + \frac{\partial \phi}{\partial s} \quad , \quad V_v = U_v + \frac{\partial \phi}{\partial v} \quad , \quad V_n = U_n + \frac{\partial \phi}{\partial n} \tag{12}$$

s and v are the non-orthogonal curvilinear coordinates defined along the streamwise and circumferential directions, respectively as shown in Figure 2. The radius increment of tip vortex cavity is determined by applying a finite difference scheme to Eqn. (11) with a periodic boundary condition at the intersection with the trailing wake, and an initial condition at the beginning of the tip vortex cavity.

- Kutta condition : The velocity at the propeller trailing edge is finite.

$$\nabla\phi < \infty \tag{13}$$

3 Wake alignment

In order to predict the shape of tip vortex cavity, first the trajectory of the tip vortex core must be determined by aligning the wake geometry with the local total velocity on the wake surface. A low order panel method is used to compute the velocity field on the trailing wake surface induced by the dipoles and sources of the system. The numerical instability in the roll-up region is avoided by calculating the induced velocity at some slightly deviated (by a distance δ normal to the wake sheet) points from the control points, as shown in Figure 3. This treatment of the roll-up region is similar to that of Krasny (1987) and Ramsey (1996), and has been found to predict roll-up shapes in 2-D which are quite similar to those of Krasny (1987). The velocity along the trajectory of the tip vortex core, $\vec{V}_{Tip}$, is evaluated by using the vector sum of the velocity vectors in the circumferential direction at each streamwise location along the tip vortex.

The induced velocity on the trailing wake panels can be computed by using the Green's formula, since the dipole and source strength on the propeller blade panels, and the dipole strengths of wake panels are already known from the previous solution. Note that the dipole strengths on the wake surface along each strip are constant in steady flow, but those strengths are convected downstream with time in unsteady flow. The induced velocity on the wake surface is given by

$$\begin{aligned} \vec{u}_{wi} &= \frac{1}{4\pi}\iint_{S_B+S_T+S_C}\left[\phi_q(t)\nabla\frac{\partial G(p;q)}{\partial n_q(t)} - \frac{\partial \phi_q(t)}{\partial n_q(t)}\nabla G(p;q)\right]dS \\ &+ \frac{1}{4\pi}\iint_{S_w}\Delta\phi_w(r_q,\theta_q,t)\nabla\frac{\partial G(p;q)}{\partial n_q(t)}dS \end{aligned} \tag{14}$$

Then, the total velocity on the wake surface is given by

$$\vec{V}_w = \vec{U}_{in} + \vec{u}_{wi} \tag{15}$$

The following numerical method was implemented to compute the aligned wake geometry which satisfies the force-free condition on the wake surface.

- steady mode ($t = 0$)

  1. Solve the steady Boundary Value Problem (BVP) with purely helical wake without any modeling of the contraction and the roll-up at the blade tip.

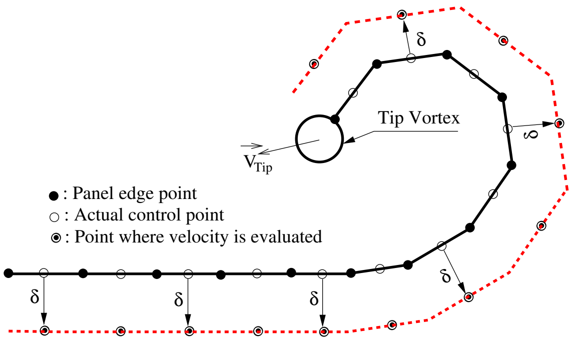

Figure 3: Definition of δ and points where the induced velocity is evaluated

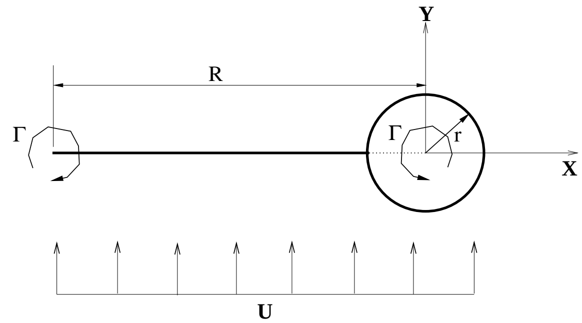

Figure 4: Modeling of 2-D tip vortex cavity

2. Once the dipole strengths on the blades and the assumed tip vortex cavity surface are known from the BVP solution, calculate the induced velocity by applying Eqn. (14) at the displaced control points.
3. Compute the mean velocity at the center of the tip vortex cavity, and interpolate the total velocity on the wake surface from those at the control points to those at the panel edge points.
4. Find the new coordinates of the wake panels by aligning with the total local velocities by using streamline equation.

$$\frac{V_w^x}{\Delta x} = \frac{V_w^y}{\Delta y} = \frac{V_w^z}{\Delta z} = \text{constant} \tag{16}$$

   where V_w^x denotes x-direction total velocity at the panel center, and Δx is the distance between two adjacent panel sides. The new coordinate at $(n+1)$th strip is determined by the following equation.

$$y_{n+1} = y_n + \frac{V_w^y}{V_w^x}\Delta x \quad , \quad z_{n+1} = z_n + \frac{V_w^z}{V_w^x}\Delta x \tag{17}$$

5. Repeat solving BVP and aligning wake geometry with updated new wake geometry until the wake geometry converges.
6. Save the wake geometry and dipole strengths on blades $(\phi(x, y, z, t = 0))$ and wake panels $(\Delta\phi(x, y, z, t = 0))$ for the unsteady wake aligning process. These steady results are the initial values for the unsteady problem, described next.

- unsteady aligning mode $(t > 0)$

1. Initially, set wake geometries of key and other blades to be the same as those in the steady mode.
2. Solve the BVP (unsteady) with the aligned wake from the steady mode. In unsteady mode, BVP is solved only for the potential of key blade and the tip vortex cavity, while the potential of other blades and potential jump of other blade wakes are assumed to be known and equal to the values on the key blade when it was located where each other blade is at the current step.
3. Compute the induced velocity on the control points of the key blade wake, and align the key blade wake geometry.
4. Solve the BVP again with aligned key blade wake and the same wakes of other blades as in (2), and determine the dipole strengths of key blade panels.
5. Save $\phi(t), \Delta\phi(t)$ and the aligned key wake geometry.
6. Move to the next time step $(t+1)$. Update the wake geometries, $\phi(t+1)$, and $\Delta\phi(t+1)$ of other blades from the previously saved data.
7. Repeat unsteady run from (2) to (6) until wake geometry converges.

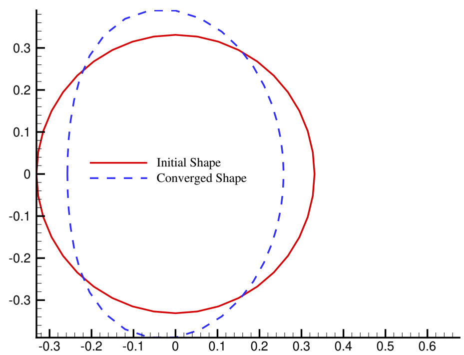

Figure 5: Comparison of tip vortex cavity shape : $\Gamma = 0.6579$, $\sigma = 0.1$, $r = 0.331$ and $U = \sin(6^o)$

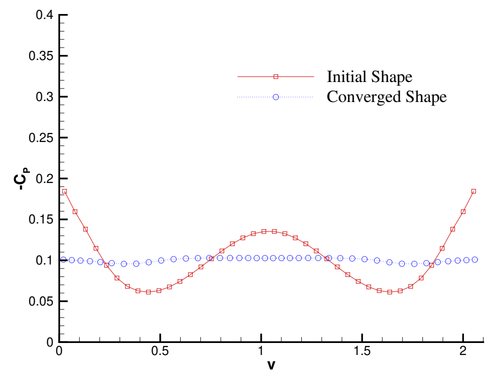

Figure 6: Comparison of pressure on tip vortex cavity surface : $\Gamma = 0.6579$, $\sigma = 0.1$, $r = 0.331$ and $U = \sin(6^o)$

- fully unsteady mode: this mode does not perform wake alignment, but uses the aligned wake as predicted in the previous mode.

  1. Update wake geometries of key and other blades corresponding to the time step t from the results of unsteady aligning mode run.
  2. Update the $\phi(t)$, and $\Delta\phi(t)$ of other blades and wakes at the corresponding time step.
  3. Repeat solving the BVP by updating $\phi(t)$, and $\Delta\phi(t)$ until the last revolution.

4 Numerical results

4.1 2-D tip vortex cavity

Starting with the simplified 2-D vortex pair, one of which has a circular initial shape, as shown in Figure 4, the tip vortex cavity shape which satisfies the dynamic and the kinematic boundary conditions, has been determined. If that vortex system is released, it will move downward due to the downwash of each vortex on the other, and this movement makes the convergence of tip vortex shape difficult. In order to avoid the movement of the vortex system, an intentional upward velocity which has the same magnitude but opposite direction to the downwash is applied on the system.

Figure 5 shows the comparison of shape of tip vortex cavity between original and converged shapes for the very strong circulation, $\Gamma = 0.6579$, $\sigma = 0.1$, $r = 0.331$ and upward velocity $U = \sin(6^o)$. The tip vortex cavity shape converges to the deformed elliptic shape from the original circle. The pressures on the initial and the converged cavity surfaces are shown in Figure 6. While the pressure is varying around the tip circumference in the case of initial shape, the converged pressure $(-C_p)$ is almost constant and equal to the cavitation number $\sigma = 0.1$.

4.2 Elliptic wing

The elliptic wing is considered to examine the wake roll-up and contraction. The cross section of the wing has a NACA66-415 shape with an $a = 0.8$ mean camber line. The maximum thickness to chord ratio, $(t/c)_{max}$ is 15%, aspect ratio $AR = 3.0$ and the angle of attack is 10^o. Figure 7 shows the converged trailing wake sheet behind an elliptic wing, where the contraction and the 3-D roll-up of the trailing wake can be seen very clearly.

In Figure 8, the tip vortex cavity trajectory computed by the present method is compared with that measured in the experiment of Arndt et al. (1991). The thick line of experimental measurements indicates the extent of variation of the trajectory for the different physical parameters such as angle of attack, Reynolds number, and cavitation number. Note that in the experiment it was observed that the trajectory did not

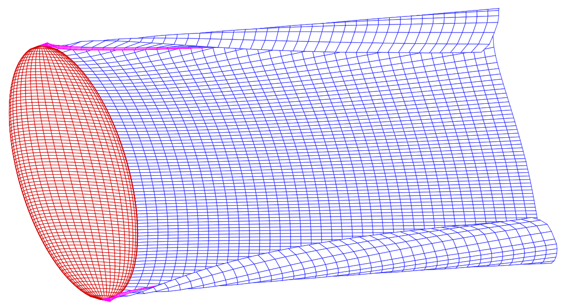

Figure 7: The converged wake geometry behind an elliptic wing : $AR = 3.0$, $(t/c)_{max} = 0.15$, and $\alpha = 10^o$

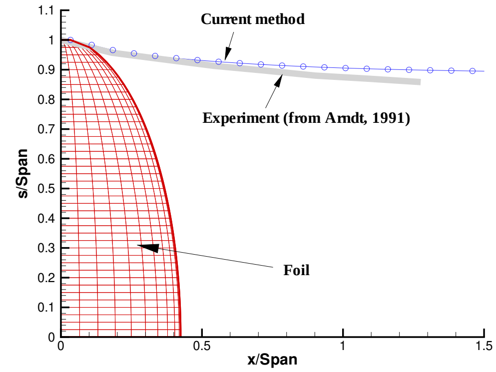

Figure 8: Comparison of the trajectory of tip vortex core with that of experiment for elliptic wing: $AR = 3.0$, $(t/c)_{max} = 0.15$, and $\alpha = 10^o$

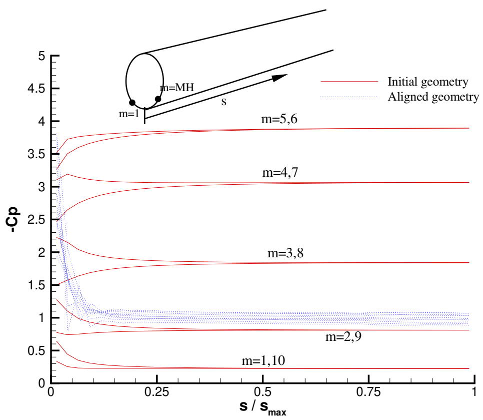

Figure 9: Comparison of pressure distributions on the original and the converged tip vortex surfaces : $AR = 3.0$, $(t/c)_{max} = 0.15$, and $\alpha = 10^o$

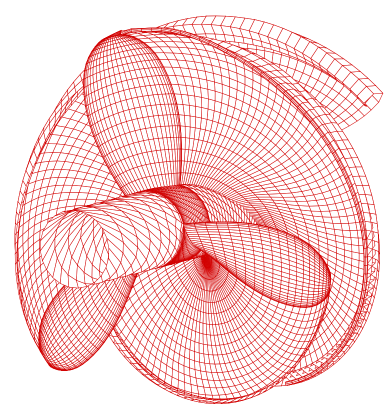

Figure 10: Geometry of DTMB4148 propeller with the fully aligned wake and tip vortex cavity : $J = 0.954$, $F_n = 9.159$ and $\sigma_n = 2.576$

depend on cavitation number, and thus the tip vortex trajectory under non-cavitating conditions can also be used under cavitating conditions. The tip vortex cavity trajectory produced by the present method (this trajectory is obtained from non-cavitating solution) agrees well with that measured in the experiment. Figure 9 shows the pressure distribution on the tip vortex surface along the streamwise direction at each circumferential strip, before and after alignment. The pressures for the aligned wake geometry are almost constant and close to the cavitation number $\sigma = 1.0$.

4.3 DTMB4148 Propeller

In order to validate the modeling of tip vortex cavity and unsteady wake alignment procedure, the shapes of blade sheet cavity are predicted[2] and compared with those of observed in the cavitation tunnel and predicted by PROPCAV [3] without modeling of tip vortex cavity.

The test conditions inside cavitation tunnel were $\sigma_n = 2.576$, $F_n = 9.519$ [4] and the advance ratio, J_s, $= 0.91$. Since this code cannot simulate the tunnel effect, the equivalence advance ratio for unbounded

[2]In this case the diameter of the tip vortex cavity is taken equal to that observed in the experiment, instead of being determined by the method.

[3]PROPCAV is a PROpeller unsteady CAVitating flow analysis code based a Boundary Element Method (Young et al. (2001)).

[4]Froude number,F_n is defined as $F_n = \frac{n^2 D}{g}$

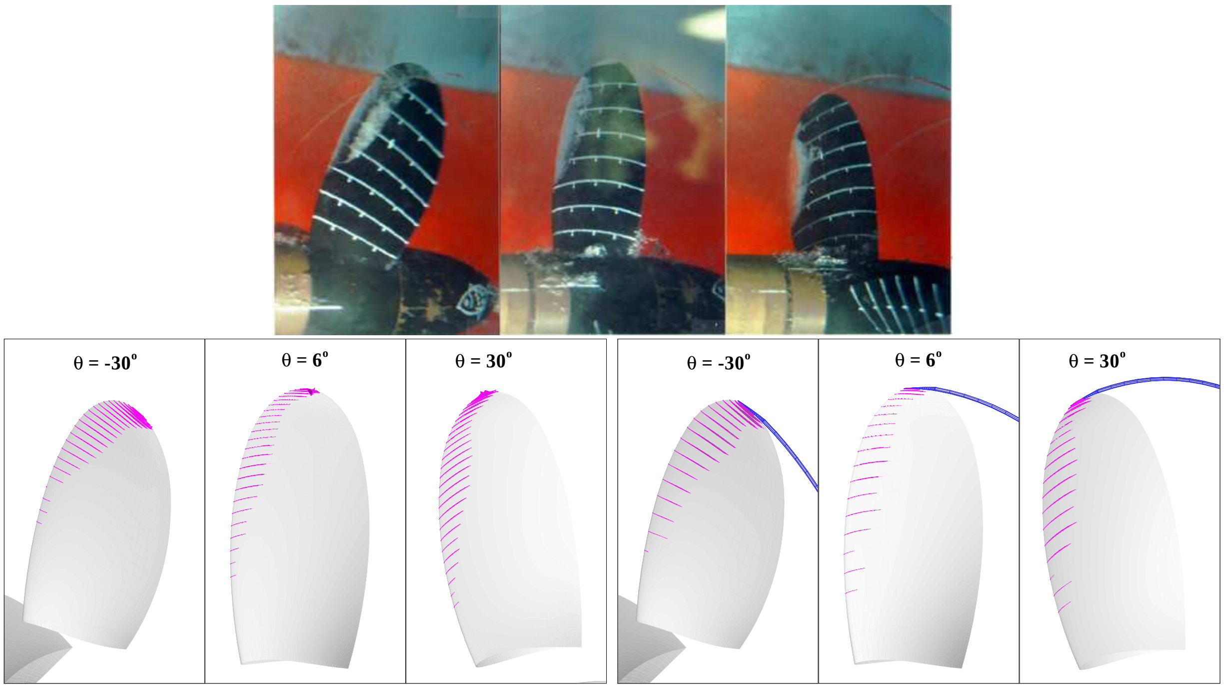

Figure 11: Comparisons of blade sheet cavities measured in the experiment(Top), predicted by PROPCAV without tip vortex model (Bottom left) and with tip vortex model (Bottom right) for DTMB4148 propeller : $J = 0.954$, $F_n = 9.159$ and $\sigma_n = 2.576$

flow was computed by matching the fully wetted trust coefficient, K_T, and found to be $J_S = 0.957$. The non-axisymmetric inflow (or *effective wake*) used in this calculation corresponds to the wake in Mishima et al. (1995) with the effects of the tunnel walls and vortical inflow/propeller interactions accounted for by using WAKEFF3D (Choi and Kinnas (1998)).

Figure 10 shows the propeller DTMB4148 and the aligned unsteady wake geometries at the key blade angle *zero* position. The aligned wake shapes of the other blades are different from each other and all show the expected contraction of the tip vortex cavity, as well the roll-up. Figure 11 shows the predicted cavity shapes compared with those observed in the cavitation tunnel and those predicted by PROPCAV without modeling of tip vortex cavity. Although the shapes of the blade sheet cavities predicted by both numerical methods agree well with those of experimental observation, PROPCAV without modeling tip vortex cavity produces unreliable (diverged) cavity shapes near the area of blade tip while the present method shows clearly converged cavity shapes at the blade tip.

4.4 DTMB4661 Propeller

The wake alignment is applied to the DTMB4661 propeller. DTMB4661 is a five bladed propeller with a moderate skew distribution. Boswell et al. (1984) performed experiments using the DTMB4661 propeller to analyze the propeller forces and moments under inclined inflow conditions. Predictions have also been provided by Kinnas and Pyo (1999) who used MPUF-3A, a vortex lattice method, in which the trailing wake sheet was adjusted by simply using the inclination angle. This code was refined recently by Lee and Kinnas (2001), where exhaustive convergence and validation tests were performed for inclined flow.

The numerical calculation is performed at the inclination angle $\alpha = 10^o$, advance ratio $J = 1.0$, Froude number $F_n = 4.0$, with both the hydrostatic and the time variations being included when solving for the fully unsteady performance. Figure 12 shows the aligned wake geometries at the varying angles of key blade positions. At each angle position, the trailing wake moves upward due to the inclined inflow and rolls up at the tip region. The projected view of aligned wakes are shown in Figure 13 where the inclination of the wake sheet is clearly shown.

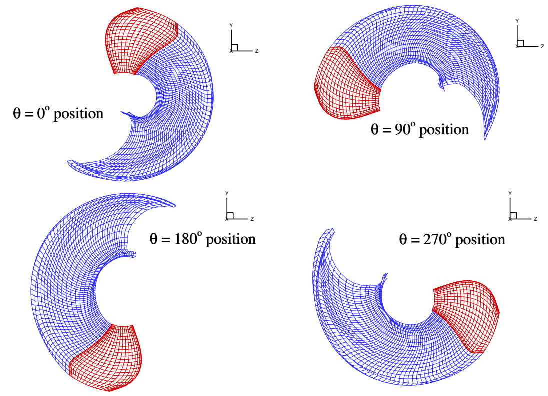

Figure 12: The key blade and aligned wake geometries for DTMB4661 propeller : $J = 1.0$, $F_n = 4$ and $\alpha = 10^o$

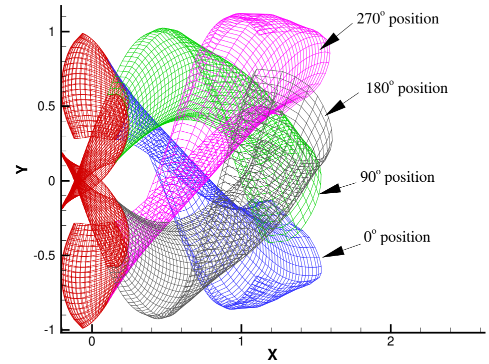

Figure 13: The projected view of aligned wake geometries for DTMB4661 propeller : $J = 1.0$, $F_n = 4$ and $\alpha = 10^o$

Figure 14 shows the amplitudes of the first harmonic of the forces acting on one blade of DTMB4661 propeller. The measured forces by Boswell et al. (1984) are also shown with those predicted by the present method and the vortex lattice method (MPUF-3A). MPUF-3A and the present method predict a similar behavior to that of the measured axial force and tangential moment. However, in the case of tangential force and axial moment, the predictions by the present method appear to be much closer to the measured than those predicted by MPUF-3A. These results indicate that fully unsteady wake alignment is required to predict accurate forces and moments when the propeller is operating in inclined inflow.

5 Conclusions

A boundary element method was applied to predict the unsteady propeller performance with blade sheet and tip vortex cavities. In the present method, the trailing wake geometry was aligned with local total velocity by applying the force free condition on each local wake panel, thus the wake geometries corresponding to the other blades are different from each other and from that of the key blade. The induced velocity was computed at a certain small distance away from the actual control points on the wake, to avoid the instability of velocity computation in the roll-up region. Although the solver for predicting the shape of the developed tip vortex cavity, which requires to satisfy the dynamic and the kinematic boundary conditions, is not fully developed yet, the results from wake alignment show that the aligning of wake geometry can improve the pressure distribution on the tip vortex cavity surface, to make it nearly uniform and close to the cavitation number.

The following applications of the present method were provided:

First, the prediction of tip vortex cavity shape was performed for the simplified 2-D vortex cavity problem. The pressure on the tip vortex cavity, as expected, was found to be constant and equal to the cavitation number.

The wake alignment procedure was applied to the trailing wake of 3-D elliptic wing to predict roll-up and contraction of wake and finally the trajectory of vortex core. The computed trajectory of vortex core for the elliptic wing agreed well with that measured in experiments.

The blade sheet cavity for the DTMB4148 propeller was predicted by applying the unsteady wake alignment method and by modeling the developed tip vortex cavity at the blade tip. The shape of the sheet cavity predicted by the present method was found to be convergent near the area of the blade tip, as opposed to that predicted without the modeling of the tip vortex cavity, which was found to be divergent.

Finally the fully unsteady wake alignment was performed for the DTMB4661 propeller rotating in inclined inflow. The computed first harmonic of the blade forces and moments for the 10^o inclination were compared with those of another numerical method (vortex lattice method with inclusion of shaft inclination) and those

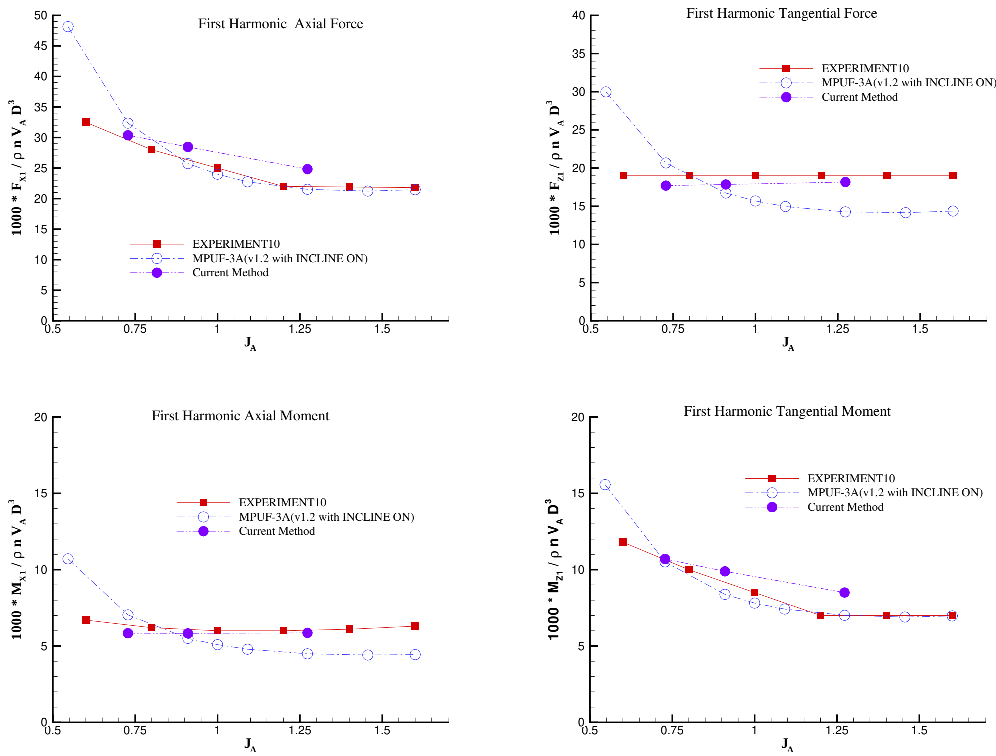

Figure 14: The first harmonic of the forces and moments acting on one blade for DTMB4661 propeller : $J = 1.0$, $F_n = 4$ and $\alpha = 10^o$

measured in the experiment. The present method was found to predict overall more accurate unsteady forces than the vortex-lattice method.

Acknowledgment

Support for this research was provided by Phases II and III of the "Consortium on Cavitation Performance of High Speed Propulsors" with the following members: AB Volvo-Penta, American Bureau of Shipping, Office of Naval Research and David Taylor Model Basin, Daewoo Shipbuilding & Heavy Machinery, El Pardo Model Basin, Hyundai Maritime Research Institute, John Crane-Lips Norway AS, Kamewa AB, Michigan Wheel, Rolla SP Propellers SA, Ulstein Propeller AS, and VA Tech Escher Wyss GMBH.

References

Arndt, R., Arakeri, V., and Higuchi, H. (1991). Some observations of tip-vortex cavitation. *Journal of Fluid Mech.*, Vol 229:pp 269–289.

Boswell, R., Jessup, S., Kim, K., and Dahmer, D. (1984). Single-Blade Loads on Propellers in Inclined and Axial Flows. Technical Report DTNSRDC-84/084, DTNSRDC.

Choi, J. and Kinnas, S. (2000). An unsteady three-dimensional euler solver coupled with a cavitating propeller analysis method. In *The 23rd Symposium on Naval Hydrodynamics*, Val de Reuil, France.

Choi, J.-K. and Kinnas, S. (1998). A 3-D Euler Solver and Its Application on the Analysis of Cavitating Propellers. In *25th American Towing Tank Conference*, Iowa City, IA.

Fine, N. (1992). *Nonlinear Analysis of Cavitating Propellers in Nonuniform Flow.* PhD thesis, M.I.T., Department of Ocean Engineering.

Fruman, D. (1994). Recent progress in the understanding and prediction of tip vortex cavitation. In *The Second International Symposium on Cavitation*, pages pp19–29, Tokyo ,Japan.

Greeley, D. and Kerwin, J. (1982). Numerical methods for propeller design and analysis in steady flow. *Trans. SNAME*, vol 90.

Kerwin, J. and Lee, C.-S. (1978). Prediction of steady and unsteady marine propeller performance by numerical lifting-surface theory. *Trans. SNAME*, vol 86.

Kinnas, S. and Fine, N. (1990). Non-Linear Analysis of the Flow Around Partially or Super-Cavitating Hydrofoils by a Potential Based Panel Method. In *Proceedings of the IABEM-90 Symposium of the International Association for Boundary Element Methods*, Rome, Italy.

Kinnas, S. and Fine, N. (1992). A nonlinear boundary element method for the analysis of unsteady propeller sheet cavitation. In *Nineteenth Symposium on Naval Hydrodynamics*, pages 717–737, Seoul, Korea.

Kinnas, S., Lee, H., and Mueller, A. (1998). Prediction of propeller blade sheet and developed tip vortex cavitation. In *22nd Symposium on Naval Hydrodynamics*, pages 182–198, Washington, D.C.

Kinnas, S. and Pyo, S. (1999). Cavitating propeller analysis including the effects of wake alignment. *Journal of Ship Research*, 43(1):pp. 38–47.

Krasny, R. (1987). Computation of vortex sheet roll-up in the Trefftz plane. *Journal of Fluid Mechanics*, 184:pp. 123–155.

Lee, H. and Kinnas, S. (2001). MPUF3A (version 1.2) user's manual. Ocean Engineering Report 01-2, Ocean Engineering Group, UT Austin, Austin, TX.

McCormick, B. J. (1962). On Caviation Produced By a Vortex Trailing From a Lifting Surface. *Journal of Basic Engineering*.

Mishima, S., Kinnas, S., and Egnor, D. (1995). The CAvitating PRopeller EXperiment (CAPREX), Phases I & II. Technical report, Department of Ocean Engineering, MIT.

Mueller, A. and Kinnas, S. (1999). Propeller sheet cavitation predictions using a panel method. *Journal of Fluids Engineering*, 121:282–288.

Ramsey, W. (1996). *Boundary Integral Methods for Lifting Bodies with Vortex Wakes*. PhD thesis, M.I.T., Department of Ocean Engineering.

Stinebring, D., Farrel, K., and Billet, M. (1991). The structure of a three-dimensional tip vortex at high reynolds numbers. *Journal of Fluids Engineering*, 113:496–288.

Young, Y. and Kinnas, S. (2001). A bem for the prediction of unsteady midchord face and/or back propeller cavitation. *Journal of Fluids Engineering*, 123.

Young, Y., Lee, H., and Kinnas, S. (2001). PROPCAV (version 1.2) user's manual. Ocean Engineering Report 01-4, Ocean Engineering Group, UT Austin, Austin, TX.